

Renormalized response function behaviour in weakly interacting van der Waals Fermi system

Sushant Kumar Behera,^{1,2,*} Prasanjit Samal,^{1,†} and Pritam Deb^{2,‡}

¹*School of Physical Sciences, National Institute of Science Education and Research, HBNI, Bhubaneswar 752050, India*

²*Advanced Functional Material Laboratory (AFML),*

Department of Physics, Tezpur University, Tezpur-784028, India

(Dated: February 12, 2023)

Weak-coupling phenomena of the two-dimensional Hubbard model is gaining momentum as a new interesting research field due to its extraordinarily rich behavior as a function of the carrier density and model parameters. Thus, there is a rapidly growing interest in the transmission of information encoded by electron and atomic spins which, in principle, can be realized by the propagation of spin waves [on account of the low-dimensional sheet structure](#). In this paper, we demonstrate the spin-wave dependent electronic structure and susceptibility behavior of model graphene-phosphorene van der Waals heterostructure in the framework of renormalization group approach. We implement Aharonov-Bohm-Coulomb-Dirac formulated field-theoretic approach for the weakly interacting Fermi system with nearest-neighbor hopping amplitudes. The analytical approach is further extended for spin-wave dependent susceptibility behavior. This finding supports the quantitative realization of experimental and theoretical systems [further](#) from their critical points before the underlying field theory is well understood for potential application.

keywords: Renormalization group theory; [vertex response function](#); [spin-wave dependent susceptibility](#); two dimensional van der Waals heterostructure; weakly interacting Fermi system;

PACS numbers: 71.10.Fd, 71.45.-d 73.63.-b, 81.05.Uw, 73.20.At

I. INTRODUCTION

Correlation effects in condensed matter many-body systems could be fundamentally described *via* Hubbard model^{1–10}. It exhibits various different channels for the transition of normal metallic behavior by an independent tunability of the electronic band structure *via* a single tight-binding parameter, *i.e.*, the interlayer hopping amplitude, and the half-filling nature on the hexagonal lattice bilayer system. In this aspect, weak-coupling phenomena of the two-dimensional (2D) Hubbard model is gaining momentum as a new interesting research field recently because of its extraordinarily rich behavior as a function of the carrier density and model parameters. In this aspect, the most promising and best controlled analytical approach is Renormalization Group (RG) theory method presently for low dimensional Fermi systems. Meanwhile, Aharonov-Bohm (AB) field potential helps in describing the details electronic and structural aspects of such systems having competing singularities at weak coupling region. Thus, combining both RG Theory *via* AB field potential frames an interesting and unique approach to realize such systems within weak coupling regime. In this regard, van der Waals (vdW) are coming under direct focus where this 2D Hubbard model can be implemented for practical realization of this method to explore the concept of spin-wave assisted field effect transistor in molecular spintronic¹¹.

To realize and analyze prototypic 2D model for the electronic degrees of freedom, Hubbard model including RG theory is promising in case of 2D planes¹². In particular, 2D Hubbard model¹³ is appropriate to ex-

plain interesting phenomena of weakly interacting systems which can be tuned by their carrier density. Besides, large scale numerical algorithms are worked out to solve such 2D interacting Hubbard model including related model parameters¹⁴. In such systems, weak interaction reveals antiferromagnetic ground state close to half-filling and symmetric *s*-wave phase away from half-filling region. In such cases, conventional perturbation theory fails at a certain region close to the half-filling region, where challenging and frequent infrared deviations raise due to weakly interacting Fermion system^{15–17} and *van Hove singularities*, [non-smooth critical points in the density of states \(DOS\) of solids in their Brillouin zone](#),¹⁸ including the AB potential field for 2D monolayer sheet system^{19–21}. Moreover, [appropriate model for 2D weakly interacting vdW Fermi systems with singularities within weakly interacting region is still lacking in the current analytical prospects](#). To overcome this fact, RG theory is presently the most efficient and promising analytical technique for such 2D weakly interacting Fermi systems^{22,23}.

Looking towards the weakly coupled vdW system prospects, atomically thin 2D materials, like hexagonal-boron nitride (h-BN), graphene (Grp) and its family, transition metal dichalcogenides (TMDCs), black phosphorous (BP), etc. are primary candidates due to their rich mechanical^{1–3}, electronic^{4,5}, optical^{6,7} and electrochemical assets with an extensive variety of promising applications^{8–10}. In recent times, multilayer vdWs heterostructures, chemically different 2D structures, have attracted recent research attention unlike monolayer pristine systems, like Grp-hBN²⁴, Grp-TMDC²⁵, h-BN-TMDC²⁶, Grp-Silicene²⁷, graphene-CrBr₃²⁸ and TMDC-

TMDC²⁹. While, many 2D materials (*e.g.* graphene and MoS₂) with efficient carrier mobilities (*i.e.* high *on-off* ratio)^{30,31} restrict their nano-dimension hetero-layer device applications. In these case, these layered 2D vdW heterostructures possess superior efficiency for carrier inoculation *via* barrier height modulation³². In this regard, phosphorene (P), a puckered honeycomb 2D material, possesses fascinating electronic³³⁻³⁵ and optical properties^{35,36}, such as finite direct band gap (~ 1.5 eV at monolayer) and high mobility ($10^3 \text{cm}^2 \text{V}^{-1} \text{s}^{-1}$ at room temperature, 300K) due to its structural anisotropy³³⁻³⁸.

In the present manuscript, we describe a semimetal-semiconductor transition and associated quantum criticality in a 2D vdW system with long-range Coulomb interaction. The role of the Coulomb interaction in 2D systems (*i.e.* $V(\mathbf{q}) \propto 1/|\mathbf{q}|$) has been widely studied with particular emphasis on graphene monolayer sheet³⁹⁻⁴⁴. As a result, the Coulomb interaction generates anomalous exponents^{41,44} at strong coupling region. However, this trend is possible only at intermediate frequency ranges as the dimensionless coupling flows towards smaller values. Moreover, the system enters into a weak coupling regime below a certain energy range. In this regime, only logarithmic renormalizations are possible⁴³⁻⁵⁰, where the quasiparticle residue tends to get a finite nonzero value at zero energy, *like*, graphene sheet preserves *Fermi-liquid* behavior at lower frequencies. As a consequence, all the possible calculations stress physical observables, like compressibility, **spontaneous diamagnetic susceptibility**, etc. by extra logarithmic parameters^{46,47,51,52}.

We implement RG theory to the 2D Hubbard model of Graphene-Phosphorene (Grp-P) heterostructure considering nearest neighbor hopping amplitudes of dense electron distribution profile close to half-filling region. Here, we particularly calculate the trend of collective two particle couplings in a single loop stage, completely ignoring the inappropriate energy and linear momentum dependency, but considering vital tangential momentum dependency being a dynamic parameter. We further extend the RG theory to obtain the susceptibility values to analyze the physical response of uncertainties gestured by diverging couplings in weakly interacting vdW heterostructure. Charge-density screening, spin-density and singlet function based susceptibilities have been considered during analytical calculations at various pairing symmetries. Here, spin-density phase diagram has been presented close to half-filling region of this 2D Hubbard model. The obtained results show the critical energy scale behavior away from the half-filling region with perfect nesting and room temperature stability of the designed system for further functionality.

II. FIELD THEORY FRAMEWORK

The Hamiltonian with the order of second quantization (H_{SQ})⁵³ unfolding the massless 2D Dirac fermions

is referred in Eq. 1 shown below,

$$H_{SQ} = \int dv \xi^\dagger(v) [v_F [-i\hbar \nabla + eA(v)] \sigma - eV(v)] \xi(v) \quad (1)$$

where, e , σ , v_F and ξ^\dagger are the electron charge, spin-wave projection, Fermi velocity and Grassmann variable, respectively (*details in Supplementary Material*⁵⁴). The Coulomb field potential originated due to the net charge of Ze positioned at the origin is $V(v) = \frac{Ze}{4\pi\epsilon_0 v}$, similarly the AB field solenoid aligned at the same point, **which** provides $A(v) = \frac{\Phi}{2\pi} (-\frac{y}{v^2}, \frac{x}{v^2})$ with a fixed total magnetic flux of Φ . Being the fixed magnetic flux, Pearl's substitution approach is limited in the flow equation. This establishes the Aharonov-Bohm-Coulomb-Dirac (ABCD) field **approach** in the present model 2D vdW heterostructure⁵⁵.

The partial wave expansion can be further expanded using rotational symmetry, which decouples the system Hamiltonian into diverse partial-wave vectors. Here, $j=(1/3), (3/2), \dots$ is the net angular momentum and we consider the dimension-free Coulomb field coupling,

$C = \frac{Ze^2}{4\pi\epsilon_0 \hbar v_F}$. Apart from the kinetic term, each radial Hamiltonian contains the Coulomb field potential and the centrifugal field potential, both of them possess scale-invariant form (*i.e.* $1/v$). Most interesting physical quantities are the charge density $\rho(v) = -e \langle \xi^\dagger v \xi(v) \rangle$ and current density $J(v) = -ev_F \langle \xi^\dagger v \sigma \xi(v) \rangle$ in the ground state of the ABCD Hamiltonian equation. The corresponding coupling presents scattering amplitude located at potential center and corresponding energy dependency **has** to be obtained using RG equations.

III. RENORMALIZATION GROUP THEORY

A. Renormalization equation formalism

We study the effects of Coulomb interaction in this 2D vdW system by combining RG theory analysis and a large N expansion. It is obvious that over a wide range of energies the screened Coulomb interaction is a relevant perturbation, and the system is in the strong coupling limit and displays non-Fermi liquid behavior with power-law energy dependence of the quasiparticle residue $Z \propto E^a$, where $a = O((\log N)/N)$. This behavior starts at $E_1 \sim \Lambda e^{-b_1 N / \log N}$, where Λ is of the order of the bandwidth and $b_1 = O(1)$, and extends down to very low energy $E_3 \sim \Lambda / (N^N)$. In the subrange $E_3 < E < E_2 < E_1$, where $E_2 \sim \Lambda e^{-b_2 N}$, $b_2 = O(1)$, the parameters of the fermionic dispersion (the velocity and the effective mass) also become energy dependent and vary as powers of E with anomalous exponents $O(1/N)$. At even smaller energies $E < E_3$, the system crosses over to weak coupling behavior. However, contrary to the case of 2D semimetals, 2D systems do not become free

particles at the smallest frequencies. Instead, in the limit $E \rightarrow 0$, the system displays marginal *Fermi liquid* behavior with universal, N -independent quasiparticle weight $Z(E) \propto (\log E)^{-3/2}$ (*details in Appendix*).

We have taken weakly interacting spin-half Fermions of single-particle basis state with crystal momentum (k_c), *up* or *down* spin-wave projection, $\sigma \in [\uparrow, \downarrow]$ and kinetic energy (E_k). Thus, the behavioral aspects of the system can be determined via following Eq. 2,

$$S[\xi, \xi'] = \sum_K (if_0 - \xi_k) \xi'_K \xi_K - \gamma[\xi, \xi'] \quad (2)$$

where, $K=(f_0, k, \sigma)$ presents a multi index parameter connecting the frequency (f_0) with each particle quantum numbers; Grassmann variables (ξ_K and ξ'_K) are allied to the formation and extinction operators, $\xi_{K=\epsilon_{K-\mu}}$ is the energy related to a particle depending on the chemical potential (μ) and $\gamma[\xi, \xi']$ is a random many body coupling factor^{56,57}.

In the calculation steps, all the connected [transient flow](#)

equations have been achieved from the functional via implementing Green's functions, given below in Eq. 3

$$G[\eta, \eta'] = \log \int \partial \mu_c [\xi, \xi'] e^{-\gamma[\xi, \xi']} e^{(\xi', \eta) + \xi, \eta'} \quad (3)$$

with the normalized Gaussian measure. [Green's function is an efficient yet accurate tool to predict the variables in flow equations and maintain proper correlation among the RG theory and ABCD field equations.](#)

The infinite hierarchy in flow equations is essential to check at a single-loop level to predict dominant structural uncertainties in the vdW system within weakly interacting limit, neglecting other irrelevant components of the effective interactions. Moreover, energy corrections of each iteration step are confined to one-particle vertex function (Γ) and used for further calculations. The spin-wave structure of Γ can be used for a spin rotation invariant system with response flow equation, which is given as follow in Eq. 4,

$$\Gamma(K'_1, K'_2; K_1, K_2) = \Gamma_s(K'_1, K'_2; K_1, K_2) \Lambda^{1/2} S_{\sigma'_1, \sigma'_2; \sigma_1, \sigma_2} + \Gamma_t(K'_1, K'_2; K_1, K_2) \Lambda^{3/2} T_{\sigma'_1, \sigma'_2; \sigma_1, \sigma_2} \quad (4)$$

where, K_1 and K_2 presents the multi indexed particle quantum numbers for both spin arrangements, singlet S and triplet T projection operators are used for two particle spin space, Λ is the energy scale varying at a functional trend for singlet and triplet operators.

B. Linear Response Behaviour

We extend the RG equations to obtain linear response behaviour (*i.e.* spin-wave susceptibility value) of the system towards finite applied external electric field⁵⁸. Finite external field (F_E) leads to an additional contribution to the action of the flow equation, which is given as follow in Eq. 5

$$\zeta[F_E; \xi, \xi'] = - \sum_q [F'_E(q) \Phi(q) + F_E(q) \Phi'(q)] \quad (5)$$

Thus, the Grassmann variables in bilinear form ($\Phi(q)$), Hermitian conjugate ($\Phi'(q)$) and $F'_E(q)$ is the complex conjugate of $F_E(q)$. One can calculate the response of the field interaction towards electronic charge density, $\rho(q) = \sum_{k, \sigma} (\xi'_{k-q, \sigma} \xi_{k, \sigma})$ and z-direction dependent spin density, $s^z(q) = \sum_k [\xi'_{k-q, \uparrow} \xi_{k, \uparrow} - \xi'_{k-q, \downarrow} \xi_{k, \downarrow}]$ and response to coupling fields which interact with the change in singlet operator, where $\partial(k)$ is an even parity function satisfying the orbital symmetry of the coupling operator (*i.e.* s wave). The linear response of the expectation value with the flow equation of the partition function $[F_E]$. Here,

the susceptibility follows like Eq. 6,

$$\chi(q) = \xi^{-1} \langle \Phi(q) \Phi'(q) \rangle_{F_E=0} \quad (6)$$

Meanwhile, translation and spin rotation invariant systems are considered with conserved charge in the absence of an external field (F_E). As a consequence, in such normal and non-symmetrical broken phase, $\langle \Phi(q) \rangle$, the expectation value nullifies at $F_E(q) \rightarrow 0$. Other physical observables, like compressibility, susceptibility, etc. are discussed in the Supplementary Material⁵⁴ in details.

IV. VERTEX FUNCTION FINDINGS

A. Vertex response function corrections

One can verify that higher-order corrections contain higher powers of l . We can either use the RG analysis, or express the full self-energy $\Sigma(\omega, \mathbf{k})$, the full vertex g , and the full polarization bubble self-consistently, via full Green's functions to get total sum of the logarithmic series, and then represent $\Sigma(l)$, $g(l)$, and $\Pi(l)$ as integrals $\int^l dl'$ over running l' to obtain RG equations by taking derivatives with respect to the upper limit⁵⁹. This can be obtained in either way the same set of RG equations for running Z , v , and A . It is obvious that the product of g and Z is not renormalized due to the conserved behaviour of electric charge. The RG equations for $Z(l)$,

$v(l)$, and $A(l)$ are ($\dot{X} = dX/dl$) as Eq. 7

$$\dot{Z}(l) = -\gamma_z(l)Z(l), \quad \dot{v}(l) = \gamma_v v(l), \quad \dot{A}(l) = \gamma_A A(l) \quad (7)$$

where $\gamma_z(l) = \gamma_z + \frac{\sqrt{15}}{\pi^{3/2}} \frac{1}{N} \log \frac{v}{v(l)}$. Solving these equations

and using $l = \log(\Lambda/E)$ we obtain $v(E)$, $A(E)$, and $Z(E)$ at energy E in the form of Eq.8

$$\frac{v(E)}{v} = \left(\frac{\Lambda}{E}\right)^{\gamma_v}, \quad \frac{A(E)}{A} = \left(\frac{\Lambda}{E}\right)^{\gamma_A}, \quad Z(E) = \left(\frac{\Lambda}{E}\right)^{-\gamma_z + \frac{\sqrt{15}}{\pi^{3/2}} \frac{\gamma_v}{N} l}. \quad (8)$$

The analysis of Eq. (7) shows that there are three energy scales characterizing the system's behavior. At high energies, $E > E_1 = \Lambda e^{-b_1 N / \log N}$, where $b_1 = O(1)$, the dependence of the fermionic propagator on E is weak, *i.e.*, fermions behave as almost free quasiparticles. **At the case of**, $E_2 < E < E_1$, where $E_2 = \Lambda e^{-b_2 N}$, $b_2 = O(1)$, v and A remain close to their initial values, but the quasiparticle residue becomes strongly E -dependent, and the fermionic propagator at the typical energy E acquires a non-Fermi-liquid form with a **random varying (i.e. anomalous) exponent** γ_z , *i.e.*, $G \propto 1/E^{1-\gamma_z}$. This behavior holds also at energies below E_2 , but now v and A grow as powers of Λ/E with anomalous exponents γ_v and γ_A , respectively. The presence of anomalous dimensions in the theory implies that physical observables, such as the compressibility, the free **and spontaneous diamagnetic** susceptibility, etc., show unusual temperature dependencies. The strong coupling results differ quantitatively, but not qualitatively from the case of graphene. In both cases, Coulomb interaction gives rise to anomalous exponents for the quasiparticle residue in the Grp-P heterostructure system.

The flow of the vertex function (Γ) and the susceptibility (χ) values have been calculated analytically using RG theory for several choices of the bare interaction, termed as the AB field potential ($U > 0$), the next nearest neighbor hopping amplitude ($t < 0$) and the chemical potential (μ), where t and μ have been fixed so that the Fermi surface and particle density are approaching to ek and half-filling (*i.e.* $n \approx 1$, $|\mu| \rightarrow 0$), respectively. Momentum dependent flow of the vertex functions are obtained for the three considered systems at low dimensional scale. It is observed that the flow of the vertex function achieves a density value ($n \approx 0.992$), *i.e.* close to half-filling region at $t=0$ and $|\mu|=0.005$ (plotted in Fig. 1). Here, the singlet part of the vertex function is taken at specified values of momenta on the Fermi surface including the values of momenta, where strong renormalization of Γ occurs. Most probably, the singlet vertex function possesses its

leading values supporting *umklapp* scattering along the diagonal direction of the k -space Brillouin zone. It is observed from the RG theory calculation that the density decreases away from half-filling (*i.e.* $n \approx 1$, $|\mu| \rightarrow 0$) region in a step-like manner and the calculations fail into a region, where s -wave symmetry dominates with pairing correlations at necessarily low scale energy levels indicating quantum confinement (*i.e.* nanostructuring) in the *Grp-P* heterostructure system. **As a result, differential step like behaviour is prominent from the plots in Fig. 1.**

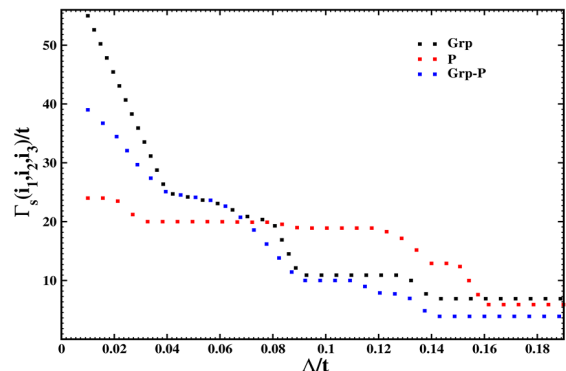


FIG. 1. Flow of the singlet vertex function, Γ , as a function of Λ for several selections of momenta values, kF_1 , kF_2 and kF_3 for the *Grp-P* heterostructure system with a comparison to the pristine graphene and phosphorene sheet. The model parameters are $U=t$ and $t=0$, and the chemical potential $|\mu|=0.005$.

B. Spin-wave dependent susceptibility behaviour

Two types of antiferromagnetic spin-wave (*i.e.* incommensurate and commensurate) susceptibilities have been obtained from the numerical calculations to validate the

physical instability associated with the diverging vertex function as a consequence of response functions^{60–62}. It is observed that the incommensurate spin susceptibilities can be neglected compared to their respective commensurate counterparts (shown in Fig. 2) due to the incommensurability parameter ($\delta \rightarrow 0$) nearing to half-filling ($n \approx 1$, $|\mu| \rightarrow 0$) as a function of energy scale. Moreover, the ratios between the two susceptibility values of monolayer system in case of weakly interacting s -wave region are in the same scale, whereas the ratios of free susceptibility are much reduced indicating the validity of response functions for 2D weakly coupled Fermi systems. In addition, the ratio in case of hetero bilayer is much greater compared to its monolayer system. Thus, antiferromagnetic wave vector based spin-wave susceptibility dominates over coupled susceptibilities at low scale energy level (*i.e.* ground state), confirming the existence of antiferromagnetic ground state with rotational spin invariance.

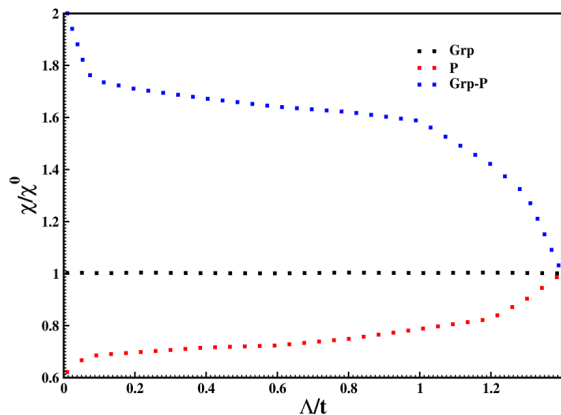


FIG. 2. The flow of the ratio of weakly interacting and free susceptibility values depending on Λ values for the *Grp-P* heterostructure system with a comparison to the pristine graphene and phosphorene sheet. The model parameters are $U=t$ and $t=0$, and the chemical potential $|\mu|=0.005$.

C. Spin-wave dependent compressibility behaviour

The values of compressibility and homogeneous spin susceptibility have been calculated depending on the energy scale (shown in Fig. 3(a) and Fig. 3(b)), respectively for the three systems. These two parameters can be realized directly from the forward scattering of vertex function *via* Landau equations of *Fermi-liquid theory*⁶³. The free compressibility, κ_0 , and spin-wave susceptibility, $\chi(s,0)$, are refined ignoring infrared cut-off values as per the *Fermi-liquid theory*. As a result, the flow equations of the vertex response function is entirely because of the flow of the Landau functions at the initial stage of the normal random phase approximation of the Hubbard

model at critical energy scale value, $\Lambda=\Lambda_0$.

The compressibility is inhibited at low scale energy

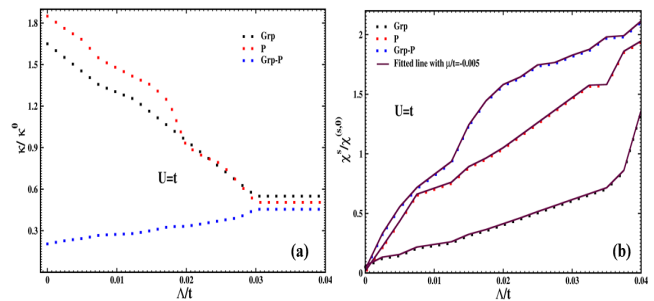


FIG. 3. The flow of (a) compressibility, κ , and (b) homogeneous spin susceptibility as a function of Λ at fixed value of $|\mu|=0.005$ for $U=t$ and $n=1$ for the *Grp-P* heterostructure system with a comparison to the pristine graphene and phosphorene sheet.

levels close to half-filling region, which is expected for systems having a finite bandgap near to μ , with dominant uncertainty in spin-wave density. Besides, the values of the compressibility diverge with respect to the reduction in homogeneous spin-wave susceptibility values away from half-filling region, where s -wave uncertainties play major role indicating a finite spin-wave bandgap opening trend in any singlet or triplet spin-wave 2D Fermi systems⁶⁴. It is found that the spin-wave susceptibility flows from zero to negative values which implies that our single loop calculation fails, when it reaches strongly interacting regime. This trend is validated only in weakly interacting region applied for 2D Fermi system. Thus, one diverging compressibility is found mentioning a strong tendency toward phase transition and separation. As a result, the increase in κ is very close to the uncertainty point, where the renormalized interactions achieve large value that the single loop findings are not further validated. The stability is prominent at higher energy scales (*i.e.* $0.04 \leq \frac{\Lambda}{t} \geq 0.03$) from the plot in Fig. 3(a) and Fig. 3(b). Moreover, we have shown the trend of free susceptibilities (χ^0) at specific choice of t and μ values (shown in Fig. 4), strongly supporting the trend of homogeneous spin-wave susceptibility.

We see that the quasiparticle residue $Z = (1 + \partial\Sigma/\partial i\omega)^{-1}$ and the parameters of electronic dispersion acquire logarithmic singular $1/N$ corrections. It is seen that the correction to Z is stronger than the corrections to v and A by $\log \alpha_N$. For the vertex correction, we find at vanishing external momentum and frequency in Eq. 9

$$\delta g_1 = -g^2 \int \frac{d^3k}{(2\pi)^3} D(k) G_0(k) G_0(k) \equiv \Sigma_\omega. \quad (9)$$

This is consistent with the calculation through out the analysis. The expression of δg_1 (shown in above Eq. 9) depends on the selection process of limit of zero momentum and frequency⁶⁵, which generally requires ex-

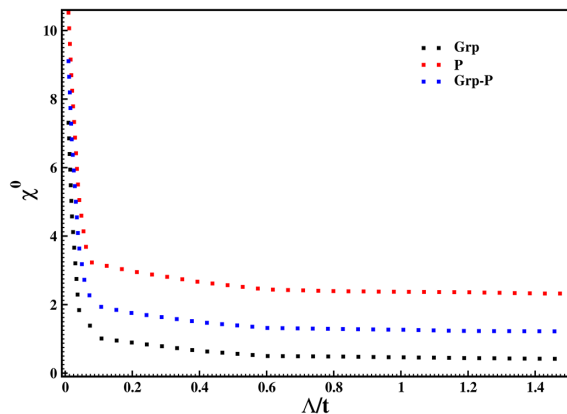


FIG. 4. Free (non-interacting) susceptibilities of *Grp-P* heterostructure system with a comparison to the pristine graphene and phosphorene sheet for $t=0$ and $|\mu|=0.005$.

tra care during the fixing process. These terms are non-logarithmic and can be safely neglected at large N values. Thus, these terms are safely skipped in our calculation set.

D. Spin-wave density dependent phase diagram

We show the phase diagram of μ and U at half-filling measured by the prevailing uncertainty from the flow equation (shown in Fig. 5(a)). The leading uncertainty region in case of *commensurate* spin-wave density is detached from the *s-wave* coupling region *via* a narrow strip where *incommensurate* spin-wave density fluctuations show dominant effect with $q=(\pi, \pi-\delta)$. For small value of U , the region surrounding half-filling is exponentially small, where uncertainties in spin-wave density play a dominant effect. The value of (t, U) , *in-plane* phase diagram is shown in Fig. 5(b) with $|\mu|=4t$ and $\mu < 0$ (below half-filling). It is observed that the chemical potential is fixed at the *van Hove singularity*^{66,67} irrespective of the value of spin-wave density, which is decreasing away from half-filling region with growing value of $|\mu|$ at 0.048, one critical point in the flow equation.

E. Behavioral trend of critical energy scale

The behavioral trend of critical energy scale, Λ_c , depending on the function at $t < 0$ where, $|\mu| \rightarrow 0$ and $U=t$ is plotted in Fig. 6(a). The shrinkage in the value of Λ_c with growing trend of $|\mu|$ confirms that the E_F residues on the *van Hove singularity* within the weakly interacting regime having only Fermi surface nesting dominance. Momentum variables of Γ have been projected upon the Fermi surfaces at specific points, where the strong renormalization of the vertex function occurs. Here, total 8 fixed points considered for the normalization process. Besides, additional 8 points have

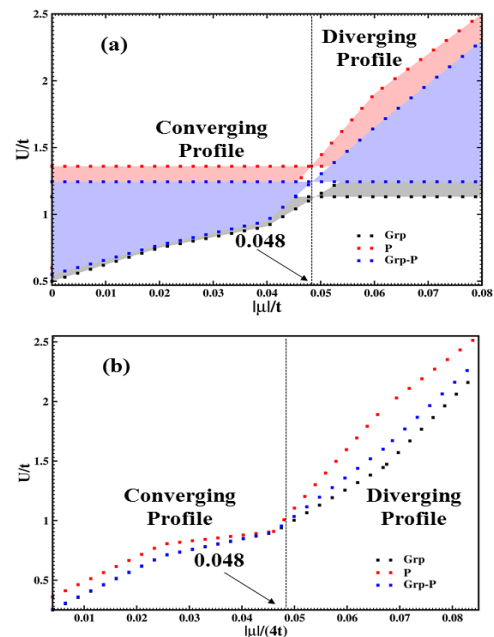


FIG. 5. Spin-wave density dependent phase diagram for (a) The (μ, U) phase diagram for $t=0$ close to half-filling ($n \approx 1$, $|\mu| \rightarrow 0$) region; the solid line represents the spin-density-wave regime of the *Grp-P* heterostructure system with a comparison to the pristine graphene and phosphorene sheet. Similarly, (b) The (t, U) phase diagram for $4t < 0$ value below the half-filling ($|\mu| < 0$) region; the dotted lines represent the spin-density-wave regime of the same three systems.

been considered in a more refined projection scheme upon the *van Hove surface* to check the collective effect. As a result, sum total 16 points (8 for *Fermi surface* and 8 for *van Hove surface*) have been taken during the flow equation calculations. These refinements, in the response function of the spin-wave density scheme, enhance the analytical calculation efficiency significantly with a reasonable reduction in critical energy scale, without altering Γ and χ values, qualitatively. The variation trend of Λ_c as a function of the inverse number of discretization points, N_0 , upon the Fermi surface at fixed choice of model parameters is shown in Fig. 6(b). It is noticed that the critical energy scale is varying in a discrete manner with 8 discretization points, and resumes stability for next 8 points with right order of magnitude indicating the controlled trend of flow equation for weakly interacting systems.

Now we obtain scaling relations for physical observables. In general, an operator O with the scaling dimension z_O obeys (as per Eq. 10)

$$O(\mathbf{k}, \omega, v, A) = z_O O(\mathbf{k}(l), \omega(l), v(l), A(l)), \quad (10)$$

where, $\mathbf{k}(l) = (z_x(l)k_x, e^l k_y)$ and $\omega(l) = z_\omega(l)\omega$ are the running momenta and frequencies. $z_{x,\omega}$ are determined by $\frac{d \log z_\omega}{dl} = 1 - \gamma_A$ and $\frac{d \log z_x}{dl} = 1 + \gamma_A - \gamma_v$. In

the case of the particle density $O = n$, $z_{O=n} = e^{-l} z_x^{-1}$. Standard scaling arguments then yield, at strong coupling, for the compressibility $\kappa = \frac{\partial n}{\partial \mu} \propto T^{1/2+\phi}$ with $\phi = \gamma_v + \frac{1}{2}\gamma_A \approx 0.4255/N$. Similarly, the diamagnetic susceptibility $\chi_{\text{dia}} \propto -T^{-\frac{1}{2}-\phi}$ ⁵². In the strong coupling regime, we immediately obtain that as per Eq. 11

$$\sigma_{x,y}(\omega) \propto N \frac{e^2}{\hbar} \left(\frac{\omega}{\omega_0} \right)^{\pm(\frac{1}{2}+\phi_\sigma)} \quad (11)$$

with $\phi_\sigma = \gamma_v - \gamma_A/2 \approx 0.299/N$. In the same manner, the weak coupling limit holds instead in Eq. 12:

$$\sigma_{x,y}(\omega) \propto N \frac{e^2}{\hbar} \left(\frac{\omega e^{\log \log^2 \frac{\Lambda}{\omega}}}{\omega_0 \log^2 \frac{\Lambda}{\omega}} \right)^{\pm \frac{1}{2}} \quad (12)$$

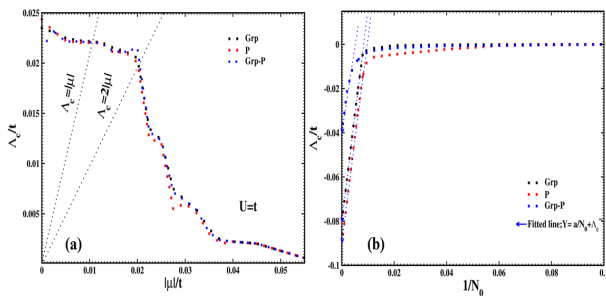


FIG. 6. The critical energy scale, A_c , as a function of (a) μ at $U=t$ and $n=1$. The dotted black lines present the functions for $A_c=|\mu|$ and $A_c=2|\mu|$ for the *Grp-P* heterostructure system with a comparison to the pristine graphene and phosphorene sheet. (b) number of discretization points, N_0 , upon Fermi surface at $U=t$, $n=1$ and $|\mu|=0.005$. The dotted black lines represent the functions $Y = \frac{a}{(N_0 + A_c)}$.

The behavior described by Eq. (13) holds as long as the dimensionless coupling $\alpha_N = (gZ)^2 N/v$ remains large. The bare value of α_N is of order N , however $v(E)$ grows upon the flow towards lower energies, and eventually, at $E < E_3 = \Lambda/N^N$, the dimensionless coupling α_N becomes smaller than one. Once this happens, the RG equations have to be modified here for proper implementation. We evaluated the one-loop self-energy and vertex corrections at small α_N and found that they are again logarithmical, but the RG parameter l is now $l = \log(E_m/E)$, where $E_m = g^2 N^2/A$ is the energy scale below which the $\sqrt{|q_y|}$ term in the polarization dominates over the bare term $|q_y|$ in the calculation. The prefactors γ_z, γ_v and γ_A are different from those other systems and are given by Eq. 13

$$\gamma_z = \frac{3\alpha_N}{8\pi^2 N}, \quad \gamma_v = \frac{\alpha_N}{4\pi^2 N}, \quad \gamma_A = \frac{\alpha_N |\log \alpha_N|}{2\pi^2 N}, \quad (13)$$

where $\alpha_N = g^2 N/v$ and gZ is not renormalized. Higher-order corrections give higher powers of logarithms, and

performing the same analysis as in the strong coupling limit, we find that $Z(l)$, $v(l)$, and $A(l)$ satisfy the same RG equations (13) as in the strong-coupling limit, but with γ 's from Eq. (14). Solving these equations we obtain at smallest energies (largest l)

$$v(l) = \frac{g^2}{4\pi^2} l, \quad Z(l) = l^{-3/2}, \quad A(l) = A e^{\log^2 l}. \quad (14)$$

We see that the quasiparticle Z does not reduce to a constant in the limit $\alpha_N \rightarrow 0$ but keeps decreasing, even at the smallest E . At the same time, we see that the series of logarithms at weak coupling do not generate anomalous dimensions, i.e., $v(l)$ and $Z(l)$ behave as powers of l (the inverse mass A has a somewhat more complex dependence on l , but still there is no anomalous dimension.) The logarithmic form of $Z(l)$ implies that the fermionic Green's function at the smallest energies behaves as $G(E) \sim (\log E)^{-3/2}/E$. Such behavior is generally termed as a *marginal Fermi liquid*. This last result shows that the weak coupling behavior of Grp-P system is *qualitatively* different from that in pristine graphene. In graphene, the quasiparticle Z factor tends to a finite value at zero energy⁴⁴, i.e. the system retains Fermi-liquid behavior with well defined quasiparticles, on the contrary, do not become sharp quasiparticles, even at the lowest energies.

V. SUMMARY AND CONCLUSIONS

A study on the spin-wave response function behavior of vdW Grp-P heterostructure was presented via field-theory perspective implementing analytical RG theory. This formulation can be used systematically to identify coupling uncertainties in 2D weakly interacting Fermi systems. In this system, critical energy can be scaled at specific singular points where vertex functions and susceptibilities diverge and become finite. **Moreover, the instabilities are modulated via short range antiferromagnetic correlations present in the system, which is noticed from the flow of vertex functions and spontaneous susceptibility. The ground state of such 2D system retains antiferromagnetic ordering accompanied with rotational spin invariance. The analytical results show an anomalous singularity of *van Hove* kind in 2D heterostructure. This finding supports the quantitative realization of theoretical systems further from their critical points and before the underlying *field theory* is well understood. This will also facilitate quantitative analysis of room temperature stability of such systems and *on-state* modeling of electronic devices in future with a step towards experimental realization.**

ACKNOWLEDGMENTS

SKB acknowledges DST, Govt. of India for providing INSPIRE PhD Fellowship (IF150325). Currently, SKB acknowledges NISER for financial support as a PDF.

Part of calculations has been performed in the KALINGA and NISERDFT HPC Facility, NISER. PS would like to thank Q-Chem, Inc. and developers for providing the source code. SKB and PD acknowledge Tezpur University for providing HPCC facility.

- * sushant@niser.ac.in, sushant@tezu.ernet.in
 † Corresponding Author(psamal@niser.ac.in)
 ‡ Corresponding Author(pdeb@tezu.ernet.in)
- ¹ Y. Nishida, *Phys. Rev. B* **94**, 085430 (2016).
 - ² A. Raju, C. B. Clement, L. X. Hayden, J. P. Kent-Dobias, D. B. Liarte, D. Z. Rocklin, and J. P. Sethna, *Phys. Rev. X* **9**, 021014 (2019).
 - ³ A. K. Geim, *Science* **324**, 1530 (2009).
 - ⁴ Y. Cai, G. Zhang, and Y.-W. Zhang, *Journal of the American Chemical Society* **136**, 6269 (2014).
 - ⁵ Y. Zhang, J. P. Small, M. E. S. Amori, and P. Kim, *Phys. Rev. Lett.* **94**, 176803 (2005).
 - ⁶ S. Qian, X. Sheng, X. Xu, Y. Wu, N. Lu, Z. Qin, J. Wang, C. Zhang, E. Feng, W. Huang, and Y. Zhou, *J. Mater. Chem. C* **7**, 3569 (2019).
 - ⁷ S. Qian, X. Sheng, X. Xu, Y. Wu, N. Lu, Z. Qin, J. Wang, C. Zhang, E. Feng, W. Huang, and Y. Zhou, *J. Mater. Chem. C* **7**, 3569 (2019).
 - ⁸ Y.-C. Rao, S. Yu, and X.-M. Duan, *Phys. Chem. Chem. Phys.* **19**, 17250 (2017).
 - ⁹ N.-N. Zhang, C. Sun, X.-M. Jiang, X.-S. Xing, Y. Yan, L.-Z. Cai, M.-S. Wang, and G.-C. Guo, *Chem. Commun.* **53**, 9269 (2017).
 - ¹⁰ S. K. Behera and P. Deb, *Phys. Chem. Chem. Phys.* **20**, 26688 (2018).
 - ¹¹ S. Z. Butler, S. M. Hollen, L. Cao, Y. Cui, J. A. Gupta, H. R. Gutiérrez, T. F. Heinz, S. S. Hong, J. Huang, A. F. Ismach, E. Johnston-Halperin, M. Kuno, V. V. Plashnitsa, R. D. Robinson, R. S. Ruoff, S. Salahuddin, J. Shan, L. Shi, M. G. Spencer, M. Terrones, W. Windl, and J. E. Goldberg, *ACS Nano* **7**, 2898 (2013).
 - ¹² Y. Hadad and B. Z. Steinberg, *Phys. Rev. Lett.* **105**, 233904 (2010).
 - ¹³ A. A. Kozikov, A. K. Savchenko, B. N. Narozhny, and A. V. Shytov, *Phys. Rev. B* **82**, 075424 (2010).
 - ¹⁴ V. P. Gusynin and S. G. Sharapov, *Phys. Rev. Lett.* **95**, 146801 (2005).
 - ¹⁵ D. Torelli and T. Olsen, *2D Materials* **6**, 015028 (2018).
 - ¹⁶ K. G. Wilson, *Rev. Mod. Phys.* **47**, 773 (1975).
 - ¹⁷ R. Shankar, *Rev. Mod. Phys.* **66**, 129 (1994).
 - ¹⁸ N. E. Bickers, D. J. Scalapino, and S. R. White, *Phys. Rev. Lett.* **62**, 961 (1989).
 - ¹⁹ N. E. Bickers, D. J. Scalapino, and S. R. White, *Phys. Rev. Lett.* **62**, 961 (1989).
 - ²⁰ A. Kumar, T. Low, K. H. Fung, P. Avouris, and N. X. Fang, *Nano Letters* **15**, 3172 (2015).
 - ²¹ D. Ebert, V. C. Zhukovsky, and E. A. Stepanov, *Journal of Physics: Condensed Matter* **26**, 125502 (2014).
 - ²² N. Furukawa, T. M. Rice, and M. Salmhofer, *Phys. Rev. Lett.* **81**, 3195 (1998).
 - ²³ M. Salmhofer, *Communications in Mathematical Physics* **194**, 249 (1998).
 - ²⁴ S. K. Behera and P. Deb, *RSC Adv.* **7**, 31393 (2017).
 - ²⁵ S. K. Behera, P. Deb, and A. Ghosh, *ChemistrySelect* **2**, 3657.
 - ²⁶ Z. Huang, C. He, X. Qi, H. Yang, W. Liu, X. Wei, X. Peng, and J. Zhong, *Journal of Physics D: Applied Physics* **47**, 075301 (2014).
 - ²⁷ M. F. Bhopal, D. W. Lee, A. u. Rehman, and S. H. Lee, *J. Mater. Chem. C* **5**, 10701 (2017).
 - ²⁸ S. K. Behera, M. Bora, S. S. Paul Chowdhury, and P. Deb, *Phys. Chem. Chem. Phys.* **21**, 25788 (2019).
 - ²⁹ G. Mills and H. Jónsson, *Phys. Rev. Lett.* **72**, 1124 (1994).
 - ³⁰ A. H. Castro Neto, F. Guinea, N. M. R. Peres, K. S. Novoselov, and A. K. Geim, *Rev. Mod. Phys.* **81**, 109 (2009).
 - ³¹ M. Y. Han, B. Özyilmaz, Y. Zhang, and P. Kim, *Phys. Rev. Lett.* **98**, 206805 (2007).
 - ³² Y. Cai, G. Zhang, and Y.-W. Zhang, *The Journal of Physical Chemistry C* **119**, 13929 (2015).
 - ³³ N. D. Mermin and H. Wagner, *Phys. Rev. Lett.* **17**, 1133 (1966).
 - ³⁴ J. Yuan, S. Najmaei, Z. Zhang, J. Zhang, S. Lei, P. M. Ajayan, B. I. Yakobson, and J. Lou, *ACS Nano* **9**, 555 (2015).
 - ³⁵ H. Liu, A. T. Neal, Z. Zhu, Z. Luo, X. Xu, D. Tománek, and P. D. Ye, *ACS Nano* **8**, 4033 (2014).
 - ³⁶ R. W. Keyes, *Phys. Rev.* **92**, 580 (1953).
 - ³⁷ M. Talukdar, S. K. Behera, K. Bhattacharya, and P. Deb, *Applied Surface Science* **473**, 275 (2019).
 - ³⁸ Y. Shi, W. Zhou, A.-Y. Lu, W. Fang, Y.-H. Lee, A. L. Hsu, S. M. Kim, K. K. Kim, H. Y. Yang, L.-J. Li, J.-C. Idrobo, and J. Kong, *Nano Letters* **12**, 2784 (2012).
 - ³⁹ A. H. Castro Neto, F. Guinea, N. M. R. Peres, K. S. Novoselov, and A. K. Geim, *Rev. Mod. Phys.* **81**, 109 (2009).
 - ⁴⁰ D. M. Basko and I. L. Aleiner, *Phys. Rev. B* **77**, 041409 (2008).
 - ⁴¹ M. S. Foster and I. L. Aleiner, *Phys. Rev. B* **77**, 195413 (2008).
 - ⁴² V. Juričić, O. Vafek, and I. F. Herbut, *Phys. Rev. B* **82**, 235402 (2010).
 - ⁴³ Y. Lemonik, I. Aleiner, and V. I. Fal'ko, *Phys. Rev. B* **85**, 245451 (2012).
 - ⁴⁴ D. T. Son, *Phys. Rev. B* **75**, 235423 (2007).
 - ⁴⁵ J. M. Murray and O. Vafek, *Phys. Rev. B* **89**, 201110 (2014).
 - ⁴⁶ D. E. Sheehy and J. Schmalian, *Phys. Rev. Lett.* **99**, 226803 (2007).
 - ⁴⁷ I. F. Herbut, V. Juričić, and O. Vafek, *Phys. Rev. Lett.* **100**, 046403 (2008).
 - ⁴⁸ P. Goswami and S. Chakravarty, *Phys. Rev. Lett.* **107**, 196803 (2011).
 - ⁴⁹ P. Hosur, S. A. Parameswaran, and A. Vishwanath, *Phys. Rev. Lett.* **108**, 046602 (2012).
 - ⁵⁰ H. Isobe and N. Nagaosa, *Phys. Rev. B* **86**, 165127 (2012).
 - ⁵¹ H. Isobe and N. Nagaosa, *Phys. Rev. B* **87**, 205138 (2013).

- ⁵² D. E. Sheehy and J. Schmalian, Phys. Rev. B **80**, 193411 (2009).
- ⁵³ J. W. Negele and H. Orland, “Quantum many particle systems,” (Addison-Wesley Reading, Massachusetts, 1987).
- ⁵⁴ S. M. describes the physical variables and related equations relating with the phase diagram of the graphene-phosphorene heterostructure system., .
- ⁵⁵ M. O. Goerbig, Rev. Mod. Phys. **83**, 1193 (2011).
- ⁵⁶ Y. Aharonov and D. Bohm, Phys. Rev. **115**, 485 (1959).
- ⁵⁷ B. J. Dalton, J. Jeffers, and S. M. Barnett, Annals of Physics **370**, 12 (2016), 1604.03375.
- ⁵⁸ K. E. Newman and E. K. Riedel, Phys. Rev. B **25**, 264 (1982).
- ⁵⁹ K. L. Hur and T. Maurice Rice, Annals of Physics **324**, 1452 (2009), july 2009 Special Issue.
- ⁶⁰ M. A. Metlitski and S. Sachdev, Phys. Rev. B **82**, 075128 (2010).
- ⁶¹ P. Bartlett, R. H. Ottewill, and P. N. Pusey, Phys. Rev. Lett. **68**, 3801 (1992).
- ⁶² S. A. Kivelson, I. P. Bindloss, E. Fradkin, V. Oganesyan, J. M. Tranquada, A. Kapitulnik, and C. Howald, Rev. Mod. Phys. **75**, 1201 (2003).
- ⁶³ S. Higashitani, Phys. Rev. B **89**, 184505 (2014).
- ⁶⁴ J.-M. Stéphan, S. Furukawa, G. Misguich, and V. Pasquier, Phys. Rev. B **80**, 184421 (2009).
- ⁶⁵ D. Belitz, T. R. Kirkpatrick, and T. Vojta, Rev. Mod. Phys. **77**, 579 (2005).
- ⁶⁶ G. Y. Chitov and D. Sénéchal, Phys. Rev. B **57**, 1444 (1998).
- ⁶⁷ V. B. Shenoy, Phys. Rev. A **88**, 033609 (2013).

APPENDIX

Renormalization group analysis

Renormalization Group method is presently the most promising and best controlled analytical approach to low dimensional Fermi systems with competing singularities at weak coupling region via Aharonov-Bohm field potential. Renormalization groups are commonly used as the existence of power-law singularities near critical points and half-filling regions. Here, the classic predictions are sometimes disturbed and logarithmic and exponential corrections are required in step-by-step process to address van der Waals low dimensional systems. To formulate the mechanism of Renormalization group theory is an interesting aspect to systematically explain the families of weakly-interacting Fermi systems united by common scaling variables. Similarly, it is worth to explain this fact comparing the existing literature and predict the non-collinear generalization for the universal homogeneous scaling of the response functions.

Now let us perform a renormalization group analysis. The effective action is given by Eq. 15

$$\begin{aligned}
S &= \int_k \psi_k^\dagger (-i\omega + Ak_x^2 \tau_x + vk_y \tau_y - \Sigma(k)) \psi_k + \int_{k,k'} ig(1 + \delta\Gamma(k, k')) \psi_k^\dagger \psi_{k'} \phi_{k-k'} + \frac{1}{2} \int_k D^{-1}(\mathbf{k}) \phi_k^\dagger \phi_k \\
&= \int_k \psi_k^\dagger (-i\omega(1 + \Sigma_\omega) + A(1 + \Sigma_{k_x})k_x^2 \tau_x + v(1 + \Sigma_{k_y})k_y \tau_y) \psi_k \\
&\quad + \int_{k,k'} ig(1 + \delta\Gamma(k, k')) \psi_k^\dagger \psi_{k'} \phi_{k-k'} + \frac{1}{2} \int_k D^{-1}(\mathbf{k}) \phi_k^\dagger \phi_k.
\end{aligned} \tag{15}$$

The action changes by rescaling as Eq. 16

$$\begin{aligned}
S &= b^{-1-z-z_2} Z_\psi^{-2} \int_{\tilde{k}} \tilde{\psi}_{\tilde{k}}^\dagger \left[-ib^{-z} \tilde{\omega}(1 + \Sigma_\omega) + Z_A^{-1} b^{-2} \tilde{A}(1 + \Sigma_{k_x}) \tilde{k}_x^2 \tau_x + Z_v^{-1} b^{-z_2} \tilde{v}(1 + \Sigma_{k_y}) \tilde{k}_y \tau_y \right] \tilde{\psi}_{\tilde{k}} \\
&\quad + b^{-2-2z-2z_2} Z_\psi^{-2} Z_\phi^{-1} Z_g^{-1} \int_{\tilde{k}, \tilde{k}'} i\tilde{g} \tilde{\psi}_{\tilde{k}}^\dagger \tilde{\psi}_{\tilde{k}'} \tilde{\phi}_{\tilde{k}-\tilde{k}'} + \frac{1}{2} b^{-2-z-z_2} Z_\phi^{-2} \int_{\tilde{k}} D^{-1}(\tilde{\mathbf{k}}) \tilde{\phi}_{\tilde{k}}^\dagger \tilde{\phi}_{\tilde{k}}
\end{aligned} \tag{16}$$

where we put tildes to represent rescaled quantities. Here we rescale the frequency and momenta as Eq. 17

$$\tilde{\omega} = b^z \omega, \quad \tilde{k}_x = bk_x, \quad \tilde{k}_y = b^{z_2} k_y \tag{17}$$

and the fields and the other parameters are rescaled as Eq. 18

$$\tilde{\psi} = Z_\psi \psi, \quad \tilde{\phi} = Z_\phi \phi, \quad \tilde{A} = Z_A A, \quad \tilde{v} = Z_v v, \quad \tilde{g} = Z_g g. \tag{18}$$

We note that D^{-1} has the same scaling dimension as k_x . The effective action keeps its form by the rescaling to be Eq. 19

$$S = \int_{\tilde{k}} \tilde{\psi}_{\tilde{k}}^\dagger (-i\tilde{\omega} + \tilde{A}\tilde{k}_x^2 \tau_x + \tilde{v}\tilde{k}_y \tau_y) \tilde{\psi}_{\tilde{k}} + \int_{\tilde{k}, \tilde{k}'} i\tilde{g} \tilde{\psi}_{\tilde{k}}^\dagger \tilde{\psi}_{\tilde{k}'} \tilde{\phi}_{\tilde{k}-\tilde{k}'} + \frac{1}{2} \int_{\tilde{k}} D^{-1}(\tilde{\mathbf{k}}) \tilde{\phi}_{\tilde{k}}^\dagger \tilde{\phi}_{\tilde{k}}, \tag{19}$$

Comparing Eqs. (18) and (19), we obtain the following relations as Eq. 20:

$$\begin{aligned}
Z_\psi^2 &= b^{-1-2z-z_2}(1 + \Sigma_\omega), \\
Z_\phi^2 &= b^{-2-z-z_2}, \\
Z_A &= b^{-3-z-z_2} Z_\psi^{-2}(1 + \Sigma_{k_x}) \approx b^{z-2}(1 + \Sigma_{k_x} - \Sigma_\omega) \approx 1 + (z - 2 + \gamma_A)l, \\
Z_v &= b^{-1-z-2z_2} Z_\psi^{-2}(1 + \Sigma_{k_y}) \approx b^{z-z_2}(1 + \Sigma_{k_y} - \Sigma_\omega) \approx 1 + (z - z_2 + \gamma_v)l, \\
Z_g &= b^{-2-2z-2z_2} Z_\psi^{-2} Z_\phi^{-1}(1 + \delta\Gamma(0, 0)) \approx b^{(z-z_2)/2}(1 + \delta\Gamma(0, 0) - \Sigma_\omega) \approx 1 + \frac{z - z_2}{2}l,
\end{aligned} \tag{20}$$

where we define γ_A and γ_v as Eq. 21

$$\gamma_A = \left. \frac{d}{dl}(\Sigma_{k_x} - \Sigma_\omega) \right|_{l=0} \approx \frac{0.1261}{N}, \quad \gamma_v = \left. \frac{d}{dl}(\Sigma_{k_y} - \Sigma_\omega) \right|_{l=0} \approx \frac{0.3625}{N}. \tag{21}$$

If we consider an observable O , we expect the scaling behavior Eq. 22

$$O(\mathbf{k}, \omega, v, A) = z_O O(\mathbf{k}(l), \omega(l), v(l), A(l)), \tag{22}$$

where z_O is the scaling dimension of the operator O , and $\mathbf{k}(l) = (z_x(l)k_x, e^l k_y)$ and $\omega(l) = z_\omega(l)\omega$ are the running momenta and frequency, respectively. z_x and z_ω obey like Eq. 23

$$\frac{dz_x}{dl} = \frac{1}{2}z_x(1 + \gamma_A - \gamma_v), \quad \frac{dz_\omega}{dl} = z_\omega(1 - \gamma_v). \tag{23}$$

Defining $b = e^l$, we obtain as Eq. 24

$$z_x = b^{(1+\gamma_A-\gamma_v)/2}, \quad z_\omega = b^{1-\gamma_v}. \tag{24}$$

The scaling behavior discussed here is only valid for $\alpha_N \gg 1$. In the weak coupling case, the low-energy physics can be obtained via naive Hartree-Fock perturbation theory with weak coupling RG analysis. Here one expects logarithmic corrections, not corrections to power law behavior.

Compressibility

In case of the particle density $O = n$, we have $z_{O=n} = b^{-1}z_x^{-1}$, such that the compressibility $\kappa = \partial n / \partial \mu$ follows $z_{O=\kappa} = b^{-1}z_x^{-1}z_\omega$. The scaling relation then implies Eq. 25

$$\kappa(T) = b^{-\gamma_v - (1+\gamma_A-\gamma_v)/2} \kappa(b^{1-\gamma_v}T), \tag{25}$$

which leads to Eq. 26

$$\kappa(T) \propto T^{1/2+\phi}, \tag{26}$$

with Eq. 27

$$\phi = \gamma_v + \frac{1}{2}\gamma_A = \frac{0.4255}{N}. \tag{27}$$

This is used for the weakly interacting systems to evaluate the compressibility factor.

Spatial conductivity

We first calculate first the bare optical conductivity. The current-current correlation function $\Pi_{\alpha\beta}(\mathbf{q}, \omega)$ ($\alpha, \beta = x, y$) for the two direction is as Eq. 28 and 29

$$\Pi_{xx}(i\Omega) = -4NA^2 e^2 \int \frac{d\omega d^2k}{(2\pi)^3} k_x^2 \text{tr}[\tau_x G(\omega, \mathbf{k}) \tau_x G(\omega + \Omega, \mathbf{k})] \tag{28}$$

$$\Pi_{yy}(i\Omega) = -Nv^2e^2 \int \frac{d\omega d^2k}{(2\pi)^3} \text{tr}[\tau_y G(\omega, \mathbf{k}) \tau_y G(\omega + \Omega, \mathbf{k})]. \quad (29)$$

We substitute $p_x = \sqrt{A}k_x$ and $p_y = vk_y$ and obtain as Eq. 30 and 31

$$\Pi_{xx}(i\Omega) = 8NA^2e^2 \int \frac{d\omega d^2k}{(2\pi)^3} k_x^2 \frac{\omega(\omega + \Omega) - p_x^4 + p_y^2}{(\omega^2 + p_x^4 + p_y^2)[(\omega + \Omega)^2 + p_x^4 + p_y^2]} \quad (30)$$

$$\Pi_{yy}(i\Omega) = 2Nv^2e^2 \int \frac{d\omega d^2k}{(2\pi)^3} \frac{\omega(\omega + \Omega) + p_x^4 - p_y^2}{(\omega^2 + p_x^4 + p_y^2)[(\omega + \Omega)^2 + p_x^4 + p_y^2]}. \quad (31)$$

The integrations over frequencies give as Eq. 32 and 33

$$\Pi_{xx}(i\Omega) = 16N \frac{\sqrt{A}}{v} e^2 \int \frac{d^2k}{(2\pi)^2} \frac{p_x^2 p_y^2}{\sqrt{p_x^4 + p_y^2}} \frac{1}{\Omega^2 + 4p_x^4 + 4p_y^2} \quad (32)$$

$$\Pi_{yy}(i\Omega) = 4N \frac{v}{\sqrt{A}} e^2 \int \frac{d^2k}{(2\pi)^2} \frac{p_x^4}{\sqrt{p_x^4 + p_y^2}} \frac{1}{\Omega^2 + 4p_x^4 + 4p_y^2}. \quad (33)$$

Since we are only interested in the imaginary part of $\Pi_{\alpha\alpha}$ on the real axis, we subtract the $\Omega = 0$ contribution and obtain Since we are only interested in the imaginary part of $\Pi_{\alpha\alpha}$ on the real axis, and thus we subtract the $\Omega = 0$ contribution. Then we obtain, Eq. 34, 35, Eq. 36 and 37

$$\Pi_{xx}(i\Omega) - \Pi_{xx}(0) = -4N\Omega^2 \frac{\sqrt{A}}{v} e^2 \int \frac{d^2k}{(2\pi)^2} \frac{p_x^2 p_y^2}{(p_x^4 + p_y^2)^{3/2}} \frac{1}{\Omega^2 + 4p_x^4 + 4p_y^2} \quad (34)$$

$$\Pi_{yy}(i\Omega) - \Pi_{yy}(0) = -N\Omega^2 \frac{v}{\sqrt{A}} e^2 \int \frac{d^2k}{(2\pi)^2} \frac{p_x^4}{(p_x^4 + p_y^2)^{3/2}} \frac{1}{\Omega^2 + 4p_x^4 + 4p_y^2}. \quad (35)$$

$$\Pi_{xx}(i\Omega) - \Pi_{xx}(0) = -4N\Omega^2 \sqrt{A} e^2 \int \frac{d^2k}{(2\pi)^2} \frac{Ak_x^2 \cdot v^2 k_y^2}{(A^2 k_x^4 + v^2 k_y^2)^{3/2}} \frac{1}{\Omega^2 + 4A^2 k_x^4 + 4v^2 k_y^2} \quad (36)$$

$$\Pi_{yy}(i\Omega) - \Pi_{yy}(0) = -N\Omega^2 v^2 e^2 \int \frac{d^2k}{(2\pi)^2} \frac{A^2 k_x^4}{(A^2 k_x^4 + v^2 k_y^2)^{3/2}} \frac{1}{\Omega^2 + 4A^2 k_x^4 + 4v^2 k_y^2}. \quad (37)$$

With $x = \sqrt{A}k_x/\sqrt{|\Omega|}$ and $y = vk_y/|\Omega|$, it follows that Eq. 38 and 39

$$\Pi_{xx}(i\Omega) - \Pi_{xx}(0) = -4c_x N |\Omega|^{3/2} \frac{\sqrt{A}}{v} e^2 \quad (38)$$

$$\Pi_{yy}(i\Omega) - \Pi_{yy}(0) = -c_y N |\Omega|^{1/2} \frac{v}{\sqrt{A}} e^2, \quad (39)$$

where c_x and c_y are numerical constants, given by It holds for $-1 < \eta < 1$ that $\Pi_{\alpha\alpha}(i\Omega) = -B|\Omega|^{1-\eta}$ leads to $\text{Im}\Pi_{\alpha\alpha}(\omega + i0^+) = B \cos(\pi\eta/2)\omega|\omega|^{-\eta}$.

Free susceptibility

We consider the spontaneous response to a field perpendicular to the plane. We use for the free susceptibility as Eq. 40

$$\chi_D = \lim_{\mathbf{q} \rightarrow 0} \frac{1}{q_x q_y} \Pi_{xy}(\mathbf{q}, \omega = 0), \quad (40)$$

with the current-current correlation function $\Pi_{\alpha\beta}(\mathbf{q}, \omega)$ ($\alpha, \beta = x, y$). The scaling dimension of Π_{xy} is z_ω^{-1} . This follows from the following logic: Using the Kubo formula and our results for the conductivity it holds that Π_{xx} has a scaling dimension $b^{-1}z_x z_\omega^{-1}$ and Π_{yy} has $bz_x^{-1}z_\omega^{-1}$. Thus, a mixed term Π_{xy} must have the geometric mean as scaling dimension, i.e., z_ω^{-1} . It leads to the scaling relation Eq. 41

$$\chi_D(T) = bz_x z_\omega^{-1} \chi_D(z_\omega T), \quad (41)$$

which yields Eq. 42

$$\chi_D \propto T^{-1/2-\phi}, \quad (42)$$

with $\phi = \gamma_v + \gamma_A/2 = 0.4255/N$.

In this case, all the steps are required for a clear understanding of the facts. As a result, rational control of individual molecular spins in nanoelectronics devices is a pivotal prerequisite to fulfill its potential applicability. Meanwhile, there is a rapidly growing interest in the transmission of information encoded by electron and atomic spins which, in principle, can be realized by the propagation of spin waves or magnetization waves through low-dimensional systems. In this aspect, weak-coupling phenomena of the two-dimensional Hubbard model is gaining momentum as a new interesting research field recently because of its extraordinarily rich behavior as a function of the carrier density and model parameters. We show that this finding supports the quantitative realization of experimental and theoretical systems farther from their critical points before the underlying field theory is well understood for potential application.